Applied Surface Science 631 (2023) 157487

Contents lists available at ScienceDirect

Applied Surface Science

journal homepage: www.elsevier.com/locate/apsusc

Full Length Article

Reactive molecular dynamics simulations of lysozyme desorption under Ar cluster impact

Samuel Bertolini *, Arnaud Delcorte *

Institute of Condensed Matter and Nanoscience, Université catholique de Louvain, 1 Place Louis Pasteur, 1348 Louvain-la-Neuve, Belgium

ARTICLE INFO

Keywords:
SIMS
ReaxFF
Gas cluster ion beams
Protein desorption
Nanofabrication
Molecular dynamics
Biofilm
Protein denaturation
Protein reactions

ABSTRACT

Using large gas cluster ion beams ($Ar^{+}_{1000\text{-}5000}$), it is possible to desorb and transfer non-volatile and active biomolecules (e.g. lysozymes, 14 kDa) for nanofabrication or mass spectrometry. Depending on the cluster and target characteristics, the collision may induce fragmentation and/or denaturation of the proteins. To clarify the Ar cluster-induced desorption mechanisms of proteins, molecular dynamics (MD) simulations were performed using reactive force fields (ReaxFF). First, lysozymes were adsorbed and relaxed on a gold surface with a (543) orientation and then bombarded by Ar clusters at 45° angle. The simulations consider different cluster sizes (from 1000 to 5000 atoms) and kinetic energies (from 1 to 10 eV/atom), investigating how these parameters affect desorption, and the concomitant chemical reactions and/or protein unfolding events. Three different surfaces were modelled: one single lysozyme adsorbed on gold, a lysozyme monolayer and a bilayer. The simulations show a correlation between the lysozyme fragmentation and the cluster energy per atom (E/n) but also an additional effect of the cluster size for a given E/n. The structure of the organic target influences the emission, which becomes softer when the amount of organic material increases. In the lysozyme bilayer, non-covalent aggregates were desorbed with relatively limited protein denaturation.

1. Introduction

Transfer of molecules from the condensed to the gas phase is central to a number of analytical and thin film fabrication methods. In mass spectrometry (ESI, MALDI, DESI, SIMS and related techniques [1–3]), (bio)molecules are extracted from the liquid or the solid phase, ionized, and transferred to a detector via electrostatic and/or magnetic lenses in the vacuum. In plasma polymerization or soft and reactive landing experiments, radicals and molecules are transferred onto a collector to create molecular and polymer-like layers and thin films. In particular, soft landing experiments allow the fabrication of coatings made of complex biomolecules such as proteins and nucleic acids by transfer of their molecular ions in the vacuum. For the applications, the quality, selectivity, and activity of the obtained biomolecular surfaces are important parameters. They depend on the film composition, the integrity of the molecules, their number, and the accessibility to their active site (e.g. enzymes) [4,5]. In comparison with solution approaches, protein soft landing constitutes an interesting alternative that avoids issues related to layer drying (protein agglomeration), deposited amount (not limited to a monolayer), or effects of competition in mixtures [6–10].

In recent years, large gas cluster ion beams (GCIB) have been applied with success to the transfer of biomolecules and proteins in the gas phase with minimal damage compared to other ion beams [11]. On the one hand, GCIB SIMS allows the analysis and localization of (bio)molecules (lipids, etc.) directly in their native environment, with a capability of high-resolution molecular depth profiling and 3D imaging [12–14]. Small proteins were also desorbed without fragmentation by large Ar clusters and their molecular ion signal detected [15,16]. Recently, protein sequencing with GCIB could even be demonstrated using a SIMS instrument equipped with an Orbitrap analyzer allowing accurate mass determination [17]. On the other hand, GCIB transfer enables the fabrication of supramolecular assemblies such as protein multilayers [18]. The first proof-of-concept experiment was reported with the transfer of lysozyme, taken as a model protein. After deposition, the transferred molecules were analyzed by ToF-SIMS, identified by sodium dodecyl sulfate-polyacrylamide gel electrophoresis (SDS-PAGE) coupled to mass spectrometry, and their enzymatic activity was measured. Taken together, the data allowed the success of the transfer to be demonstrated, and in particular that an important fraction of the transferred

* Corresponding authors.
E-mail addresses: samuel.bertolini@uclouvain.be (S. Bertolini), arnaud.delcorte@uclouvain.be (A. Delcorte).

https://doi.org/10.1016/j.apsusc.2023.157487
Received 17 February 2023; Received in revised form 27 April 2023; Accepted 7 May 2023
Available online 17 May 2023

protein molecules conserved their bioactivity [19]. Therefore, the use of GCIB to transfer (bio)molecules opens new perspectives to construct biofilms without the use of solvents.

The initial protein transfer experiments were conducted using a primary beam of Ar cluster ions with a size distribution centered around 5000 atoms and an acceleration energy of 10 keV (10 keV Ar^{+}_{5000}). Indeed, previous experimental studies showed that an energy per atom of the beam around 2 eV/atom or lower caused the desorption of molecules with minimal fragmentation [20–22]. A monotonic decrease of molecular dissociation with decreasing *E/n* in the 1–10 eV/atom energy range was also demonstrated by further experiments, using ToF-SIMS analysis of angiotensin and neurotensin transferred on silicon collectors [18]. In parallel, experiments of Ar cluster-induced desorption with Irganox 1010 [20] and benzylpyridinium samples at 45° incidence provided insights into the average kinetic (KE) and internal energies (IE) of the sputtered molecules [21]. Our experiments demonstrated that below 10 eV/atom, the axial KE of Irganox molecular ions dropped, as did the IE transferred to smaller benzylpyridinium ions [21]. The IE distributions estimated by Fu and Brunelle [21] using the survival yield method, showed that the ions emitted by Ar clusters with low *E/n* have internal energies comparable to those produced in MALDI and ESI, which are recognized to be soft ion formation methods. Although extremely high pressures and temperatures are transiently reached upon cluster impact [23,24], the emission process is very fast (picoseconds), apparently preventing molecular dissociation. However, the mechanistic details of desorption, the influence of the nature of the system (molecule adsorbed on metal or in an organic layer), the dependence on the impinging cluster parameters (size, energy, incidence angle) and the effect of the desorption process on the tri-dimensional structure of the bio(macro)molecules remain incompletely understood. To go further in that direction, beyond experimental approaches, our knowledge should benefit from the ongoing development of cutting-edge modelling methods and massively parallel computing platforms.

From the computer modelling viewpoint, molecular dynamics (MD) already contributed tremendously to the elucidation of fundamental questions of sputtering and desorption [25–29], including the bombardment of surfaces with large clusters [28,30–34]. MD simulations of the bombardment of an organic surface have indicated the capacity to desorb intact macromolecules (60 kDa) [35], and reactive force fields, enabling bond scissions and formations, were also used to describe molecular GCIB of CH_4 and CO_2 [35–37]. In particular, ReaxFF proved to be adequate to describe the sputtering of polystyrene and polymethyl methacrylate with a single formalism for all the involved interactions [29]. Using a bond order formalism, the ReaxFF method can describe reaction phenomena within classical molecular dynamics [37–41] and has been applied to diverse fields, such as batteries, combustion, and catalysis [38,42–44]. Another important application regarding the subject of our study is the use of ReaxFF for protein interactions. Indeed, the force field has been trained for several amino acids and peptides, including their interactions with gold [45–48]. Additionally, improvements of ReaxFF allow the force field to explicitly treat electrons [49–51] and calculate London dispersion forces [52], which suggests possibilities to simulate ions in a semi-classical approach.

In this article, we performed ReaxFF MD simulations, first to elucidate the desorption and fragmentation of a single protein (lysozyme 1GXV [53]) adsorbed on a gold surface after the impact of a large Ar cluster, then to investigate the desorption process from an organic thin film (monolayer and bilayer). Modelling such complex systems, that simulate Ar as GCIB colliding with proteins on a gold surface, to the knowledge of the authors, is a novelty. Therefore, different sizes for the Ar cluster (from 1000 to 5000 atoms) and a range of kinetic energies (up to 50 keV) were systematically explored to better understand the desorption and fragmentation mechanisms of adsorbed proteins. The simulations suggest that lysozyme can be desorbed of a gold surface with and without fragmentation, depending on the cluster size and its velocity. A cluster with *E/n* smaller than 2 eV/atom tends to not fragment the protein, while fragmentation increases with the size and *E/n* of the Ar cluster. The desorption process is also affected by the organic motif on the Au surface, and the increase in the organic layer thickness reduces fragmentation and allows more proteins to be desorbed, including non-covalent clusters.

2. Computational methods

The molecular dynamics simulations of argon cluster impacts involving protein targets were performed using the ReaxFF [39–41] force field implemented in the Large-scale Atomic/Molecular Massively Parallel Simulator (LAMMPS) code [54,55], where the charge equilibration is calculated by the electronegativity equalization method (EEM) [56]. All the ReaxFF parameters used to calculate the pair interactions were trained by Zhang et al. for C/H/O/N/S; the interaction between Au and the other elements were parametrized by Monti et al.; and Ar interactions with the atoms‘ system were trained by Kamat et al. [45,57,58]. In the force fields, the bond parameters between N-S and O-S were not taken into account because there are no such bonds in the starting molecules trained in the force field. Therefore, in our simulations, the force field neglects the possible formation of N-S and O-S bonds, which could result in some artifacts. However, given the scope of our study and the small number of S atoms in the lysozyme molecule (1GXV [53]), these should have a minor effect on the results.

More generally, ReaxFF can under or overestimate the energy of a reaction, which could lead to favoring preferential reactions during the collision between the Ar clusters and the proteins. In the collision between two atoms, as described by Urbassek et al. [34,59] and Postawa et al. [37], the Ziegler–Biersack–Littmark (ZBL) potential [60] is used to improve the repulsive barrier energy of ReaxFF. Comparing the bond energy dissociation profile of C-H in benzene and C-H as pair interaction (**Figure S1**), the ZBL potential improves the repulsive barriers, particularly for pair interactions. Nonetheless, the energy barrier also changes accordingly to the surrounding atoms, in a competition between the bond and repulsive energies, as it also occurs in ReaxFF. For example, in the case of C-H or C-C in benzene, ReaxFF can better describe the energy barriers than the pair C-H (**Figure S1**). Considering that ReaxFF better mimics the energy barriers for bigger molecules, the mobility of the atoms in the protein collectively gaining kinetic energy, and the rather soft nature of the interatomic collisions (<10 eV/atom), we ponder that the absence of an added repulsive energy barrier (e.g. ZBL potential) minimally affects the desorption and fragmentation of the proteins. To substantiate these considerations, the simulation of single protein desorption from gold after the collision with Ar_{3000} was also conducted using the ZBL potential appended to ReaxFF. The ZBL potential was tabulated as described by Postawa et al. [61] with the R1 and R2 values as listed in **Table S3**, where R2 is the distance where the ReaxFF or ZBL forces approaches zero. The comparison between the simulations performed with or without ZBL potential for the highest energy/atom in our system (6–10 eV) indicated very similar effects, trends and final results. Therefore, the simulations presented in the article do not include the ZBL repulsive potential. The energetic changes during the reactions of our simulations are sufficiently large and can be reasonably described by the ReaxFF method with negligible artifacts. Finally, the version of ReaxFF developed for proteins appeared to be the most appropriate to account for the complexity of our systems containing gold and lysozyme.

For all the bombardment simulations, spherical argon clusters were built from an Ar crystal with space group Fm-3m and lattice parameter 5.25 Å, with the exact amount of 1000, 2988, and 5017 Ar atoms (1000, ~3000, ~5000). The Ar clusters had an initial temperature set to 10 K (using random velocity vector orientations) and additional translational velocity was added to the atoms. Because the Ar potential parameters contain only repulsive interactions, no relaxation was conducted for the Ar clusters prior to the impact simulations. The incidence angle of the clusters with respect to the surface was 45°, which is a common (and

optimal) angle used for sputtering [62] and secondary ion mass spectrometry experiments [63]. Although the center of the Ar cluster depends on the cluster size, the cluster was set close to the surface and distant enough from the protein, enabling the cluster to collide first with the Au surface. All the calculations used a time step of 0.1 fs.

2.1. Bombardment of a single lysozyme adsorbed on gold

The first system, a single protein adsorbed on a gold substrate, was set using an Au slab of 160 × 165 Å, without periodic boundary conditions (Fig. 1). This system comprising one single molecule was considered ideal to isolate the influence of the Ar cluster parameters (size and energy) over the desorption and fragmentation processes. The impacts of clusters with different sizes (number of atoms of Ar in the cluster) and collision energies were computed (see Table 1).

Prior to the bombardment simulations, the lysozyme structure was relaxed at 300 K during 14 ps. Each relaxation sequence was pursued for a few picoseconds beyond the point where the total system energy started oscillating around a constant value. Additionally, all the relaxation procedures were simulated in a NVT ensemble using Nosé-Hoover thermostat [64–66], while the collisions used an NVE ensemble with a Langevin region on the gold slab. During relaxation, there was a small change in the protein volume (from 16,776 to 16,588 $Å^3$), but no significant change in its structure. All the initial bonds and hydrogen bridges remained the same, including the 5 water molecules initially confined inside the protein. A gold crystal, with space group Fm-3m and lattice parameter of 4.078 Å, was cleaved along the direction (5 4 3) allowing the surface to contain step defects with (1 1 1) terrace orientation. The relaxed protein was then set without contact on top of the Au substrate after its relaxation, allowing the surface to adsorb the protein and stabilize the structure at 300 K for 10 ps. A total of six random orientations were tested, and the most stable structure was selected for further bombardment simulations. While the protein was being adsorbed onto the gold substrate, there were changes only in the weak interactions, giving a total adsorption energy of 12 eV (~0.01 eV/$Å^2$). Thus, the residues at the periphery of the lysozyme were attracted by the gold atoms and the area of contact between the protein and the substrate increased over time up to a maximum. The tertiary structure of the protein showed some degree of distortion, but the final configuration remained quite close to the initial structure of the lysozyme (**Figure S2**).

For the bombardment simulations, one Au layer was frozen to represent the bulk structure, three Au layers were set as a Langevin damping region to reduce backward pressure wave propagation induced by the Ar cluster collision, with the initial and final temperature set to 300 K and 100 fs of damping [67,68]. Six Au layers were left free to move. The same protocol (frozen and Langevin layers) was applied to the slab sides. The Ar cluster was initially set so that the distance between the center-of-mass of the molecules and the cluster is approximately equal to the cluster diameter when the cluster touches the Au surface. All the bombardment simulations were run for a total of 20 ps. For simplicity, the cluster kinetic energy (E) divided by the number of atoms in the cluster (n) will henceforth be called atomistic kinetic energy or E/n.

Table 1
Argon cluster parameters for the collision on a gold substrate with an adsorbed lysozyme.

Cluster size (atom)	E/n (eV/atom)	Total Kinetic energy (keV)
1000	1.0	1.0
1000	2.0	2.0
1000	4.0	4.0
1000	6.0	6.0
1000	10.0	10.0
3000	1.0	3.0
3000	2.0	6.0
3000	4.0	12.0
3000	6.0	18.0
3000	10.0	30.0
5000	1.0	5.0
5000	2.0	10.0
5000	4.0	20.0
5000	6.0	30.0
5000	10.0	50.0

2.2. Bombardment of a protein layer

Two other systems were set up in order to investigate effects related to the increasing coverage of the substrate by the proteins. To simulate a single organic layer, lysozymes were added to cover the surface, with different degrees of rotation in order to maximize the surface coverage yet avoiding overlapping proteins, and the system was relaxed at room temperature. The relaxation process induced some aggregation of the proteins, as is also observed experimentally, resulting in an incomplete coverage of the surface. However, this sample will be called lysozyme "monolayer" throughout the article for simplicity. The second organic film, coined the "bilayer" sample, was obtained by adding an equivalent number of proteins on top of the monolayer sample with the same logic

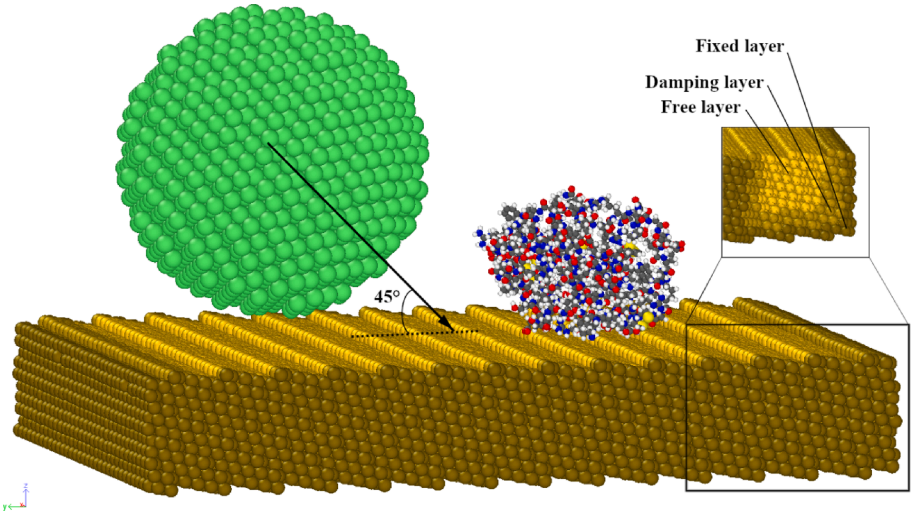

Fig. 1. Initial model structure used to investigate a single protein desorption from a gold surface after collision with an Ar cluster. The gold slab is surrounded by two Au layers, one for damping the pressure waves, and another frozen to represent bulk gold. Color code: H is white, C is gray, N is blue, O is red, S is yellow, Ar is green and Au is golden. The damping and fixed layers have darker contrast, and the frozen layer is darker than the damping layer.

of trying to maximize coverage, then it was relaxed again. Because of the step-by-step protocol used and the protein aggregation phenomenon, heterogeneities remained in both mono and bi-layer samples. However, there are differences in the Au slab structure of the organic monolayer and the bilayer. For the lysozyme monolayer, the slab dimension was 180 × 180 Å, while the number of frozen, Langevin damping, and free Au layers were: 1, 3, and 6, respectively. For the lysozyme bilayer, the slab dimension was 240 × 240 Å, with 1 frozen Au layer, 1 layer of Langevin damping Au atoms, and 3 layers of free Au atoms. It was not possible to achieve a gold surface large enough to totally eliminate the edge effects of the slab on the behavior of lysozyme molecules, as will be seen in the results section. Nevertheless, the bilayer cell was made larger than the monolayer, increasing the available area that can be affected by cluster collision, reducing the edge effects and optimizing the capability to desorb lysozymes. Though we were careful to express conclusions that should also remain valid for larger samples, our systems should be seen as nanoparticles rather than infinite gold surfaces with adsorbed proteins. For the interaction between Ar clusters and the monolayer, three impacts were computed, with cluster sizes of Ar_{3000} with *E/n* of 4.0 eV/atom, and Ar_{5000} with *E/n* of 3.0 and 4.0 eV/atom. In the case of the bilayer, only one impact of Ar_{5000} with a kinetic energy of 3.0 eV/atom was calculated (Fig. 2). In both simulations, the total time was 30 ps. Considering 15 keV Ar_{5000} as reference, only two variables change: The thickness of the organic layer or the velocity of the cluster.

3. Results and discussion

3.1. Dynamics of the protein desorption

With the selected impact parameters (incidence angle and aiming point), the clusters impinge on the side of the adsorbed lysozyme, a situation that was found optimal for molecular desorption in our previous simulations [35]. Fig. 3 shows the time-evolution of the impact of a 18 keV Ar_{3000} with the gold-supported lysozyme, in order to illustrate the general features of the dynamics of protein desorption upon bombardment by large gas clusters. Upon impact, the Ar cluster is compressed on the gold surface (Fig. 3 at 0.5 ps). In turn, a fraction of the Ar atoms in collision with the gold gains kinetic energy parallel to the surface, so that they further hit the protein and eventually lift it up from the surface. In parallel, the side of the spherical cluster directly hits the lysozyme, which becomes compressed at the collision front (Fig. 3 at 1.1 ps). Eventually, through the combined action of the Ar atoms backscattered from the gold and those directly hitting the molecule side, the protein is ejected from the surface. During the desorption process, the adsorbed region of the protein slides and rolls on top of the gold surface, inducing denaturation. The defects present on the gold surface help to trap part of the protein, promoting bond breaking (Fig. 3 at 1.6 ps). Most of the lysozyme is eventually desorbed from the gold surface, except for a few small fragments that tend to stick to it.

During the collision of the Ar cluster and the surface, it is possible to characterize the fragmentation process by computing the number of generated species. The larger is the number of species, the more extensive is the fragmentation of the protein. The fragmentation is more pronounced at the beginning of the simulation, mainly during the first 3 ps, that is the period of collision and desorption (Fig. 3). This is best described by computing the number of fragments formed as a function of time (Fig. 4). During the desorption period (2–3 ps), the fragmentation rate, defined as the derivative of the fragment number per unit of time, grows exponentially, while after desorption, reactions continue to occur at a much slower rate (Fig. 4A).

For the analysis of the bond breaking and bond formation processes, each bond is counted if the distance between two atoms is smaller than the cut-off distance of their respective bond type (**Table S1**), otherwise, the pair is considered as not bonded. Due to the effect of internal kinetic energy (temperature of each molecule), the number of bonds oscillates over time but follows an average (Fig. 4). The numbers of C-O and C-S bonds remain quite constant over the simulation (they decrease by only one unit), Fig. 4B. The time-dependence of the fragment number is correlated with the break of C-C, C-N, and S-S bonds (Fig. 4**-C**, **D,** and **E**). Three out of four S-S bonds are broken during the desorption process. Meanwhile, 12 % and 4 % of the N-C and C-C bonds get severed. In contrast, the net numbers of N-O, O-H, N-N and S-H bonds increase during the simulation time, indicating new bond formation.

At the beginning of the interaction, hydrogen atoms are removed from the protein and implanted in the gold slab (**Figure S3**), while others migrate into the protein and fragments. The hyperthermal hydrogen radicals, which interact with the gold surface and penetrate the slab and end up creating interstitial defects (which in a real metal causes hydrogen embrittlement, a common metallurgical phenomenon [69,70]). Experimentally, implantation of hydrogen in gold can be induced by ultra-sonic waves [71], which should constitute a softer interaction than the collision with the keV Ar clusters in our study. On the other hand, the low solubility of hydrogen in gold at low temperatures [72,73], indicates that interstitial H atoms in gold are not thermodynamically favored and so they tend to disappear from the surface with time. In our simulations, ReaxFF underestimates the repulsive barrier for Au_6-H (Fig. S1A), and as a result, channeling of the H atoms into the slab might be overestimated. However, H atoms were also implanted into the slab in the simulation where a ZBL potential was appended to ReaxFF. Since the ZBL potential tends to overestimate the repulsive energy barrier with respect to DFT (Fig. S1A), we suspect that in that case H implantation in the slab might be underestimated.

As a result of H transfer inside the protein, the numbers of O-H and S-H bonds increase over time (from ~32/0 to ~38/5 respectively). In parallel, the number of C-H bonds decreases until it stabilizes after 12 ps of simulation, constituting the main source of H atoms for further reactions. S-S bond breaks are associated with the formation of new S-H bonds, while the formation of the O-H bonds is a consequence of the change in the double bond to a single bond between C and O. The time-dependence of the number of N-H bonds is peculiar. At the beginning of the collision (first 2 ps), the Ar cluster removes H atoms from the N-containing residues of the lysozyme, and part of these stay on the gold.

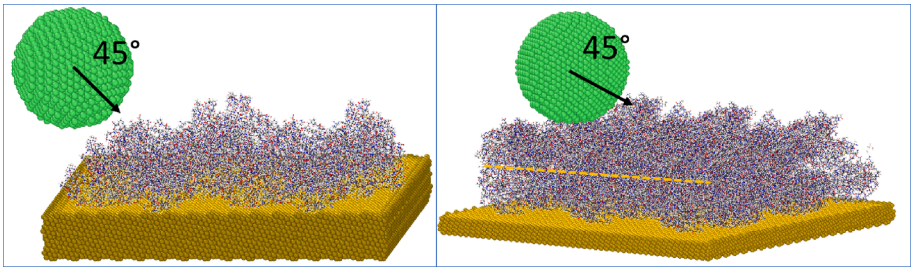

Fig. 2. Initial model structure used to study the collision of Ar clusters with a monolayer and bilayer of lysozyme adsorbed on a gold surface. Color code: H is white, C is gray, N is blue, O is red, S is yellow, Ar is green and Au is golden. The damping and frozen layers have darker contrast, and the frozen layer is darker than the damping layer.

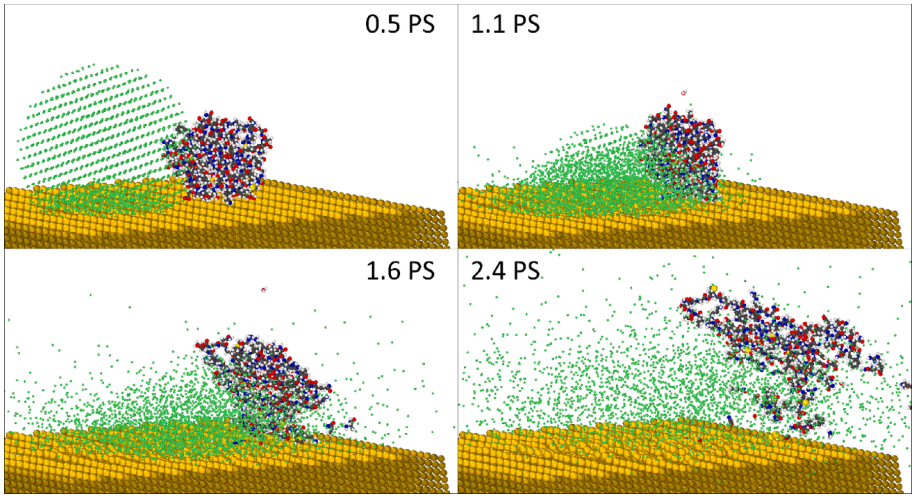

Fig. 3. Time-evolution of the desorption of lysozyme from the gold surface, using Ar_{3000} and $E/n = 6.0$ eV/atom. Color code: H is white, C is gray, N is blue, O is red, S is yellow, Ar is green and Au is golden.

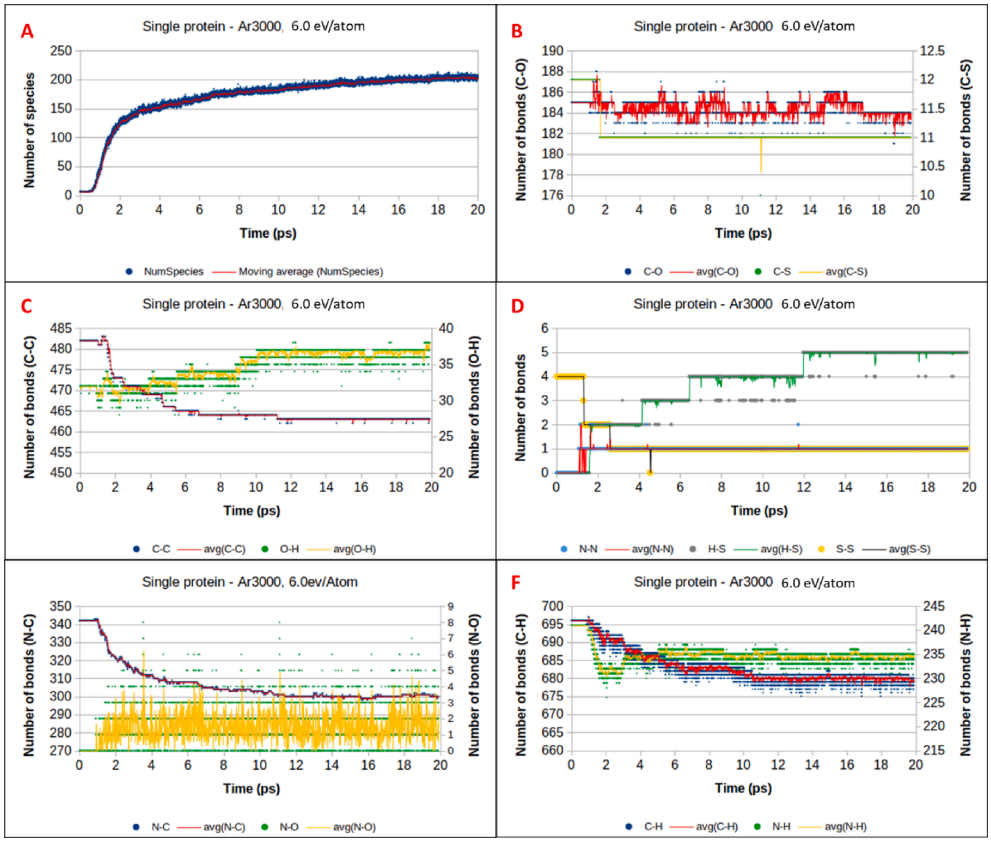

Fig. 4. Time-evolution of the total number of species (fragments) and number of bonds for each bond type upon bombardment of lysozyme with Ar_{3000} at 6.0 eV/atom. A) Total number of species; B) Numbers of C-O and C-S bonds; C) Numbers of C–C and O–H bonds; D) Numbers of N-N, H-S, and S-S; E) Number of N-C and N-O bonds; and F) Numbers of C–H, and N–H bond.

After the beginning of the collision (2 ps), C-H bonds become the source of H to other atoms (N, O, and S) and the number of N-H bonds increases again. One N_2 is formed at the beginning of the collision, due to a break in the N-H and C-N bonds. The molecules structures that are formed will be supplied under request.

Analyzing the pair interactions with gold during the protein compression regime (up to 1.5 ps), the number of bonds involving Au slightly increases, except for S that decreases (Fig. S4A). After the compression regime (from 1.5 ps) the molecule starts desorbing and the number of bonds between Au and C/N/O decreases, while those involving S increase again. The number of Au-H pairs starts to increase after 1.0 ps and keeps increasing (Fig. S4B). During this period, a number of H atoms are removed from the surface and migrate in the gold slab (**Figure S3**). The fast increase of the Au-H bond number is an indication that hydrogen can be easily removed from the protein. The cut-off distance for bonding with Au is shown on **Table S2**.

3.2. Effect of the energy per atom (E/n) of the projectile

To obtain a better understanding of the effect of the atomistic kinetic energy (E/n) of the Ar cluster projectile, we now concentrate the analysis on impacts with Ar clusters of the same size, namely Ar_{3000}, and varying total kinetic energies (see Table 1). First, the protein is desorbed from the gold surface in all the collisions with Ar_{3000}, irrespective of E/n (from 1.0 to 10.0 eV/atom). After the collision, water molecules are also removed from the protein tri-dimensional structure. When the E/n value of Ar_{3000} is 1.0 or 2.0 eV/atom, the protein is ejected from the surface without real dissociation (Fig. 5). Nevertheless, hydrogen abstraction reactions are observed, the lysozyme having one H atom removed when E/n is 1.0 eV/atom, and two H atoms removed when E/n is 2.0 eV/atom. In this low energy range, the reactions happen with the atoms close to the Au surface, because part of the protein rolls on top of the gold before desorption, so that the adsorption forces help to induce H abstraction. Adsorption forces are indeed larger on the step defects at the edges of the (1 1 1) terraces, due to the lower coordination of gold atoms. Covalent bonds involving H tend to be weaker than other covalent bonds such as C-C and C-N and non-covalent hydrogen bridges are even more labile, so they can be severed with a lower E/n. The quasi-intact protein removed from the surface at these low energies can be totally or partially denatured. However, denaturation does not seem to be directly correlated with the E/n value, because in our simulations, when the protein is more denatured for the 1.0 eV/atom than for the 2.0 eV/atom impact (Fig. 5). Nevertheless, a larger number of simulations should be computed in the

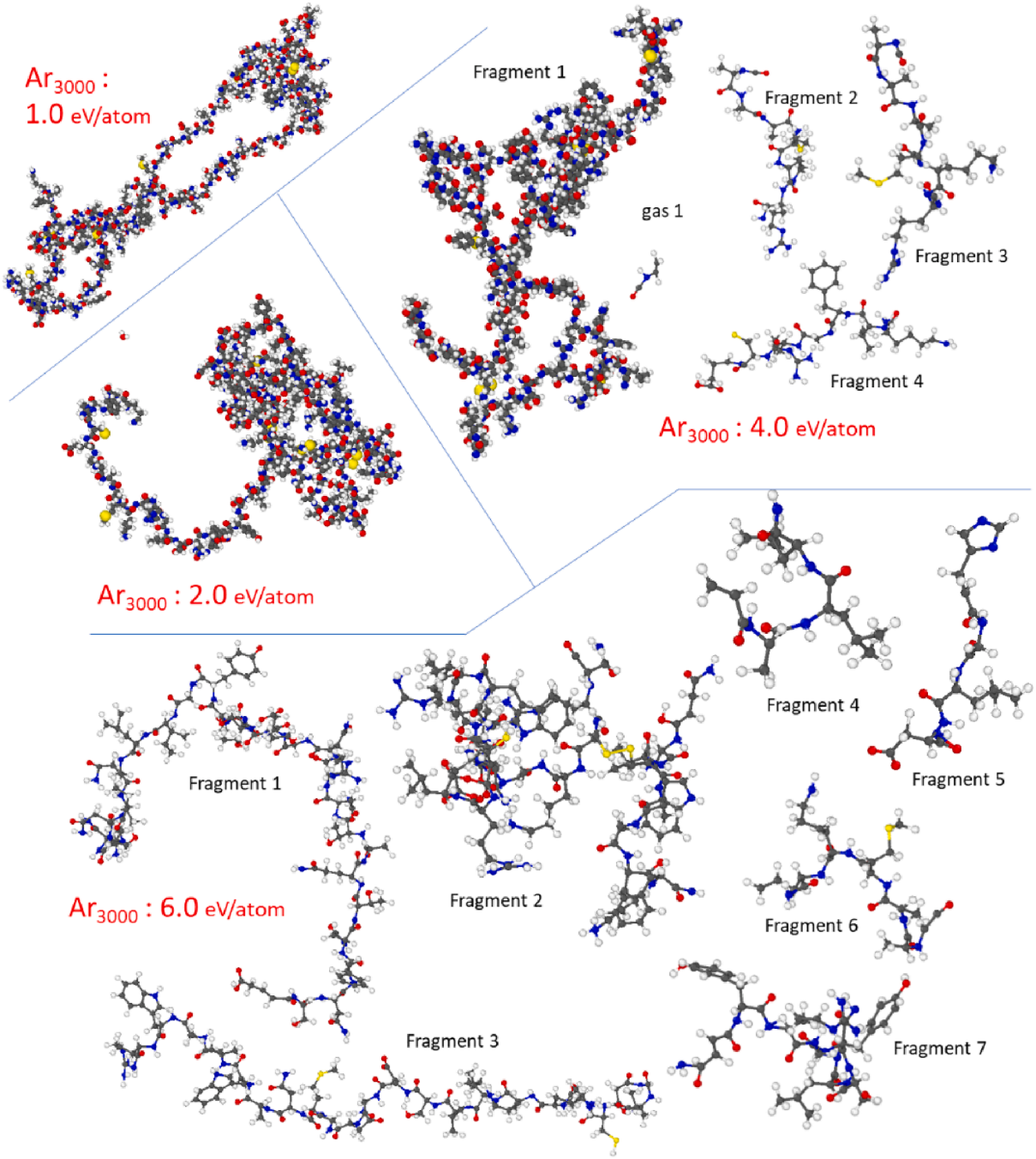

Fig. 5. Image of the desorbed lysozyme or its biggest fragments formed after the collision with an Ar_{3000} cluster with increasing atomistic kinetic energy (E/n = 1.0, 2.0, 4.0, and 6.0 eV). The fragments were randomly numbered. Color code: H is white, C is gray, N is blue, O is red, S is yellow.

low energy range to definitely conclude on this point. Our results suggest therefore that denaturation tends to be more a statistical effect, instead of being directly influenced by the cluster E/n.

When the atomistic kinetic energy increases, for example at E/n = 4.0 eV/atom, one of the fragments formed is large, indicating that only part of the protein is heavily damaged (Fig. 5). For E/n values above 4 eV (e.g. 6 eV), fragmentation generally increases and the fragments become smaller (Fig. 5). The protein's primary structure is largely destroyed, generating amino acids and small peptides in a gas state. The time-evolution of the fragment number is similar for E/n equal 4.0, 6.0, and 10.0 eV/atom (**Figure S5**), but with a different rate of fragmentation that makes the curve rise proportionally to the E/n value. Larger E/n values induce higher numbers of fragments during the collision/desorption events and in the beginning of the fly time (after 4 ps). Note that a number of radicals may also react on the fly while colliding with other fragments or they simply continue to break down into smaller fragments.

3.3. Effect of the total kinetic energy of the projectile

The simulations indicate that the atomistic kinetic energy of the cluster (E/n) determines the mechanism of emission, promoting either intact desorption or fragmentation of the protein. Here, we investigate the influence of the cluster size and how it can affect the emission, by comparing the impacts of Ar_{1000}, Ar_{3000}, and Ar_{5000} on lysozyme. The first effect of the cluster size is in their capacity to desorb the protein from the gold surface. Except for Ar_{1000} with E/n = 1.0 eV (**Figure S6**), all the other clusters were able to remove the lysozyme from the surface. In the case of 1 keV Ar_{1000}, part of the denatured protein sticks to the surface, which makes the molecule rotate towards the surface in a way that would prevent its emission at later times. A similar effect was observed for keV cluster-induced polystyrene oligomer desorption form a polymeric surface [35]. Therefore, one can conclude that emission becomes problematic below 1 keV.

The 3D plots of Fig. 6 allow us to represent the effects of E/n (Energy per atom) and of the cluster size in a single graph, in order to separate the relative contributions of these two parameters. For the same E/n = 4.0 eV in Fig. 6A, fragmentation seems negligible for Ar_{1000} but significant for Ar_{3000}. With E/n = 6.0 eV, the number of fragments at 20 ps for the clusters Ar_{1000}, Ar_{3000}, and Ar_{5000} are 25, 80, and 107, respectively. Nevertheless, irrespective of the cluster size, there is no fragmentation for E/n < 2.0 eV/atom. Considering a linear interpolation of the points, the partial derivative of the expected number of fragments with respect to E/n, is several orders of magnitude larger than the derivative with respect to the cluster size, which suggests a threshold-like behavior along E/n and a smooth variation along the cluster size axis. Note that the results can be better interpolated with a polynomial equation (Fig. 6A). Nevertheless, the rate of fragmentation is larger for Ar_{5000} than Ar_{1000} at a given E/n. In first approximation, the distribution of the heaviest emitted fragments at 20 ps (Fig. 6B) can also be fitted with a sigmoidal function of E/n but, in fact, the size of the heaviest fragment also decreases with increasing cluster size at high E/n, which shows the limits of the fit. Though the data seem to indicate a E/n threshold between 2 and 4 eV/atom, an additional effect of the cluster size is demonstrated. To our knowledge, this separate effect of cluster size on fragmentation at a given E/n is reported here for the first time.

In order to find elements of explanation for these observations, the processes of cluster impact and shattering on the surface were analyzed in more detail. As was illustrated in Fig. 3, part of the Ar atom flux is blocked by the protein. Interestingly, a fraction of the Ar atoms preferentially scatter on the sides of the lysozyme, with velocities sometimes exceeding the velocity of the cluster before backscattering (Fig. S7A). At

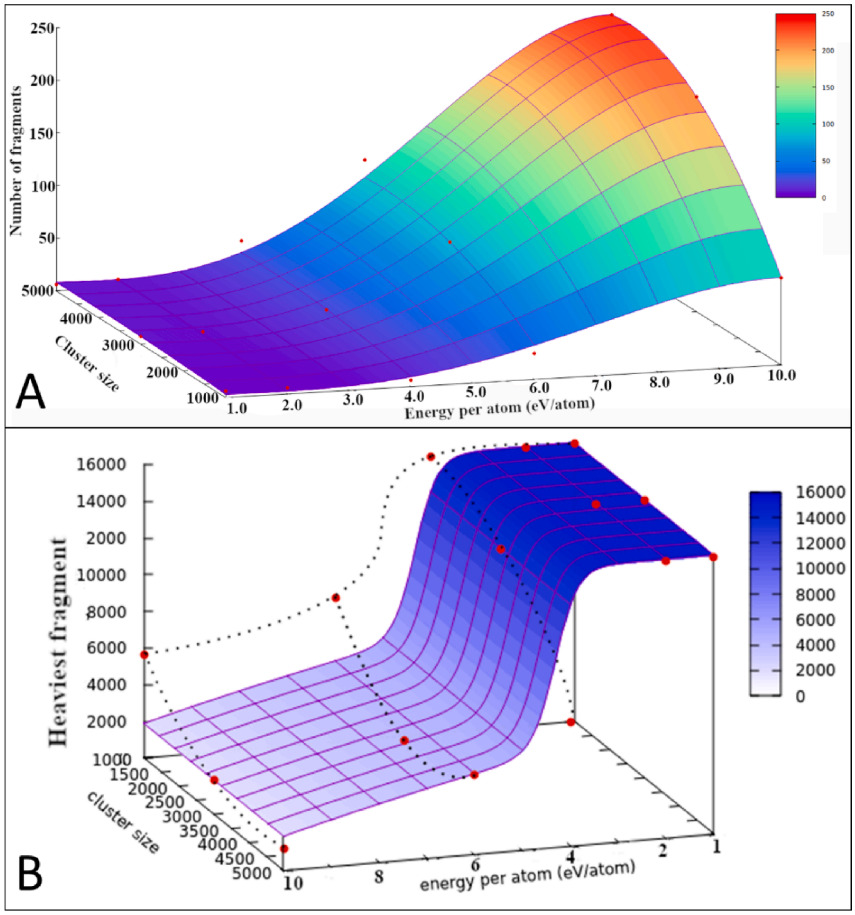

Fig. 6. Fragmentation of lysozyme and its correlation with the Ar cluster parameters (size and atomistic kinetic energy) at 20 ps. A) Number of fragments formed accordingly to the Ar cluster parameters as red points, and an interpolated colored surface scaled by the number of fragments. B) Mass of the heaviest fragment (Da) that survives after fragmentation of lysozyme, with respect to the cluster parameters as red points, an interpolated colored surface scaled by the value of the heaviest fragment, and an interpolated dashed-line for better fitting.

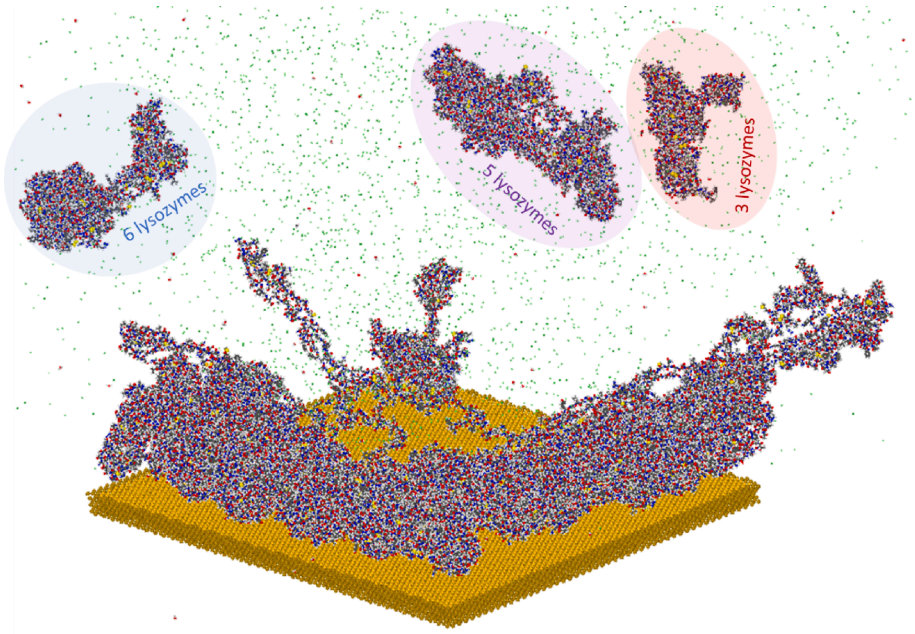

Fig. 7. Desorption of a lysozyme bilayer upon 15 keV Ar_{5000} bombardment (3.0 eV/atom). Snapshot of the time evolution at 30 ps after the impact. Color code: H is white, C is gray, N is blue, O is red, S is yellow, Ar is green and Au is golden.

the end of the simulation (20 ps), the atom kinetic energies follow gaussian distributions (Fig. S7B). The standard deviations of the distributions for $Ar_{1000\text{-}5000}$ impacts with 6.0 eV of energy per atom are relatively similar (3.9 eV), but the averages vary: Ar_{1000} is 3.84 eV, Ar_{3000} is 4.17 eV, and Ar_{5000} is 4.45 eV. The distributions also confirm that many Ar atoms are accelerated upon impact ($E/n > 6.0$ eV) and that the absolute number of these accelerated atoms increases significantly with the cluster size.

It can be rationalized that, for fragmentation to occur, the energy of individual Ar atoms impinging atoms from the protein should be sufficient to promote bond-breaking. Therefore, a correlation with the cluster E/n is expected. In parallel, the number of atoms that can promote bond-breaking and protein atoms recoiling is proportional to the cluster size. On the other hand, looking at the impinging cluster as a single entity with a given translational energy, one could argue that a large cluster (equivalent or larger than the molecule size) should be more able to transform its energy in center-of-mass kinetic energy of the desorbing protein, rather than in internal energy inducing bond-scissions (correlated push). In our simulations, the Ar atom angular and energy distributions upon and after impact show that the initial correlation of the Ar atom motions is already lost when desorption occurs. In addition, the collision can accelerate certain atoms to a significantly larger kinetic energy than the initial average E/n and the number of atoms backscattered with high energies increases proportionally to the cluster size (Fig. S7B). These effects explain the observation that the number of fragments increases with the total projectile kinetic energy E.

3.4. Desorption from an organic layer

In order to study the effect of the amount and structure of the adsorbed organic material on the desorption process, and thereby attempt to generalize the conclusions deduced for the desorption of an isolated lysozyme, a reduced number of impacts were computed for samples consisting of a monolayer and a bilayer of lysozyme on gold. Fig. 7 shows a perspective view of the molecular desorption from a lysozyme bilayer bombarded by 15 keV Ar_{5000}. With that energy, the whole organic layer is disturbed and several molecules are desorbed, mainly as non-covalent clusters containing 6, 5, and 3 lysozymes. The projectile atoms wash the organic material away from the impact point, so that the center of the gold slab is left bare at the end of the event. When the argon cluster collides in an organic monolayer or bilayer, the Ar atomistic kinetic energy profile looks different than the one previously observed for a single lysozyme in **Figure S7**. In the case of the isolated molecule, the Ar atoms have no barriers on the side preventing their reacceleration upon backscattering off the Au surface. In contrast, the full organic layers provide an organic wall in every direction, allowing the Ar cluster atoms to escape only from the top of the protein layer (Fig. 8). As a result, the profile of the Ar atom front becomes more spherical as the organic layer thickness grows. During the collision, the proteins are dislocated from their initial positions, exposing the Au surface and creating a wall of lysozymes, that is "taller" in the bilayer than in the monolayer. With the increase of the organic layer thickness, the interface between the Ar cluster atoms and the proteins becomes more vertical and the velocity vectors of the backscattered Ar atoms diverge from the surface.

The organic layer structure also influences the fraction of ejected lysozymes. In the monolayer, only the proteins close to the impact region are desorbed from the surface (**Figure S8**). And the desorption occurs not only in the axis of the collision but also in the lateral directions. In general, some large fragments may remain adsorbed on the surface. However, the capacity to remove molecules and their fragments from the Au surface is also proportional to the Ar cluster size for a given E/n (4 eV/atom in **Figure S8**). After the collision with Ar_{3000}, only the proteins immediately around the impact point are ejected, while the circle grows with Ar_{5000}. Also, the size of the fragments remaining adsorbed tends to decrease when the cluster size increases. In the bilayer, the desorbed lysozymes were initially close to the impact region as it was observed in the monolayer but, they essentially come from the top layer (**Figure S9**). Another difference with the bilayer system is that the desorption of the proteins occurs mainly in the ballistic direction of the Ar cluster, while in the monolayer the desorption was more multi-directional (**Figure S10**). However, an influence of the heterogeneity of the protein layer structure on the specific emission pattern is to be expected, since the characteristic dimensions of these heterogeneities are not negligible with respect to the impinging cluster size.

While the cluster penetrates the bilayer, proteins are dislocated more easily from the top layer than from the bottom layer. Part of the energy of the cluster is spent to move the top layer proteins away. The motion of

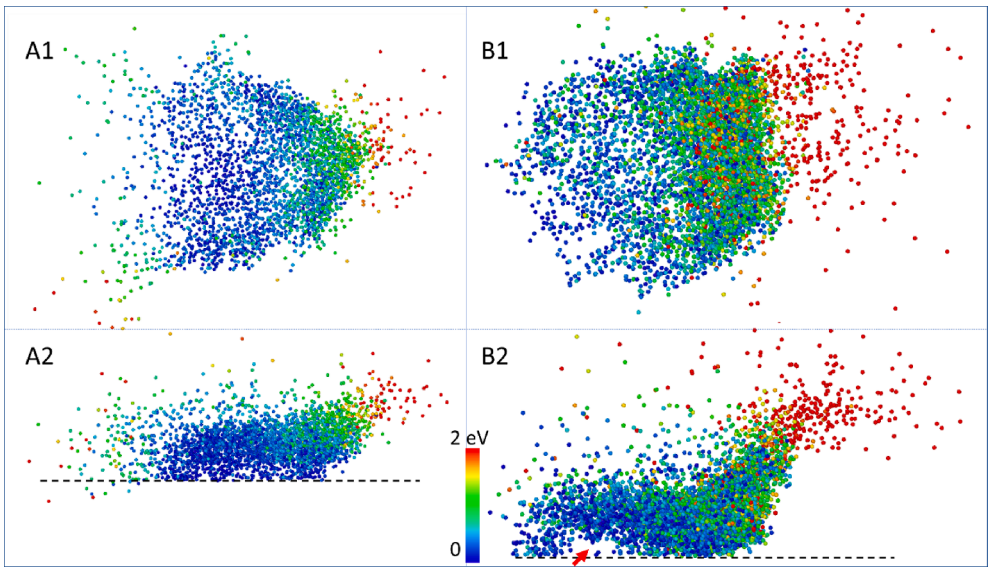

Fig. 8. Kinetic energy distributions of Ar atoms at 5 ps of simulation in different profile views (1-top, 2-side). A) Collision on a lysozyme monolayer, B) Collision on a lysozyme bilayer.

the bottom layer of proteins is constrained by both their interactions with the gold slab and with the other proteins all around. Overall, the Ar atoms supply more energy to the organic layer for molecular motion and desorption, this is indicated by the change in kinetic energy in the proteins, where the thicker is the organic layer, the larger is the change in the kinetic energy of the protein (**Figure S11**). Nevertheless, the interaction exposes the bare Au surface even for the bilayer system. This suggests that the Ar cluster could penetrate even deeper into the surface if the organic layer was thicker. This is consistent with previous MD simulations, including the 10 keV Ar_{1000} bombardment of a bulk phenylalanine sample by Mücksch et al [34]. Another important difference that can be observed with the bilayer, is the tendency to reduce protein denaturation upon emission and also to favor the desorption of protein aggregates (see Fig. 7).

As was shown before (Fig. 5), the direct collision between an Ar cluster with $>$ 3 eV/atom and a protein induces fragmentation, however, differences are also observed depending on the organic adsorbate structure. For the isolated protein, the majority of the fragments are ejected from the surface (Fig. 3). In the protein monolayer, the collision generates a number of fragments that remain adsorbed at the surface. In the bilayer, the fragments of proteins sitting on top of the surface are sputtered easily, while the other fragments created from the compression of the proteins in contact with the Au slab stay in the surface. The effect of the compression can be seen in the kinetic energy profile of Ar atoms (Fig. 8). Indeed, a curvature appears at the location of the compressed protein (Fig. 8 red arrow), where the Ar cluster atoms do not reach the Au slab.

The effects of the cluster *E/n* and size on the fragmentation of the single protein adsorbed on gold are also observed for the lysozyme monolayer. The number of small fragments increases with *E/n* (4.0 vs 3.0 eV/atom in Fig. 9-**A**) for the same cluster size (Ar_{5000}). The fragmentation also increases with the Ar cluster size (Ar_{5000} vs Ar_{3000}) at constant *E/n* (4.0 eV/atom in Fig. 9-**A**). These confirmations of our previous results indicate that the desorption of an isolated protein from an Au surface, less computationally intensive, can be used as a qualitative reference for simulations and experiments (**Figure S12**). However, in quantitative terms, our data show that the fraction of emitted fragments decreases with increasing amount and thickness of the organic layer, i.e. when going from a single molecule to an adsorbed monolayer and then to a bilayer (see Fig. 9-**B**). This effect is reminiscent of the increase of fragmentation experimentally observed for decreasing polymer layer thicknesses [74].

Another important question is whether the fragments formed as a result of the collision can react with other molecules of the organic layer. In the case of the Ar_{3000} bombardment of the monolayer (at 4.0 eV/atom), a close examination of the data indicates the formation of a molecule heavier than the lysozyme after impact. Precisely, one fragment formed during the collision is able to react with an intact lysozyme

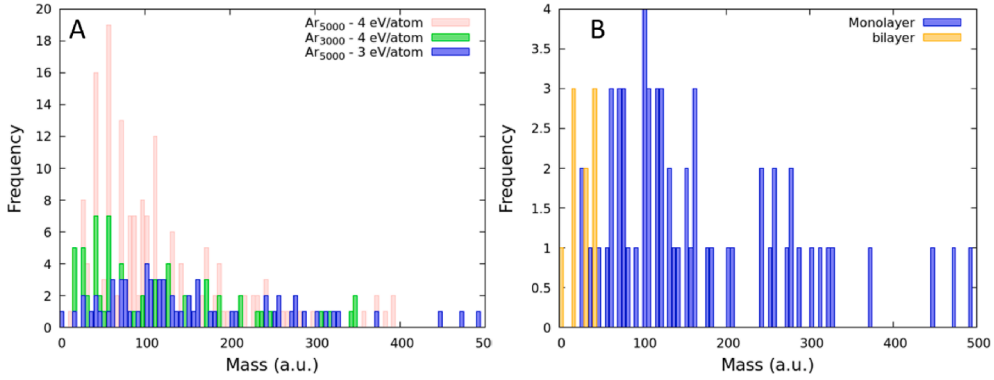

Fig. 9. Mass distribution of lysozyme fragments in the range 0–200 Da as a function of the Ar cluster parameters (size and atomistic kinetic energy). A) Bombardment of a lysozyme monolayer with different Ar clusters; B) Comparison between a monolayer and a bilayer using Ar_{5000} at 3.0 eV/atom.

that remains eventually attached to the surface (Fig. 10-**A,B,C**). Fragments and intact lysozymes can thus react, the lysozyme and the fragment staying connected by the creation of a CO bond, that is triggered by an undercoordinated C present in the fragment. Eventually, a new structure of the type R-O-C-R is formed. This confirms that the fragments surviving on the surface are reactive and suggests that they will tend to modify the surface over time and/or after repeated bombardment.

When several proteins are present on the surface, the impact can ablate H atoms from a protein, which then migrate and react with other proteins. Often, the reaction occurs with a CO termination resulting from previous fragmentation or H ablation (Fig. 10D). The migration of H is frequently observed and affects both the desorbed proteins and the proteins that remain attached to the surface. However, the proteins on the fly either fragment without reacting with other proteins or fragments (unimolecular dissociation), or they remain intact (agglomerated or not). The observation of unimolecular dissociation reactions after desorption for these short computation times indicates that fragments should probably further react on the fly, or even upon impact with the collector in transfer experiments.

Finally, when *E/n* increases sufficiently to dislocate atoms from the Au slab, they may attach to the desorbing protein or fragments. The removal of Au atoms together with proteins was observed in the case of isolated lysozyme bombardment as well as for the protein coatings (see **Figure S13**). Typically, the removal of Au atoms from the slab is associated with the presence of S in the proteins, because of their strong affinity. However, it is not correlated with the cleavage of the disulfide bonds.

3.5. General discussion and link with experiments

Our simulations indicate that it is possible to transfer lysozyme in the vacuum using large gas clusters without damaging the primary structure of the protein. This is consistent with recent experimental observations [19], which demonstrated that a significant fraction of lysozymes could be transferred by 10 keV Ar^+_{3000} and Ar^+_{5000} ions with, in addition, retention of their biological activity. However, the MD also predicts that partial or total denaturation occurs, at least when the protein is desorbed from the gold substrate with atomistic energies in the 1–2 eV/atom range. In comparison, the results obtained with lysozyme bilayers (Fig. 7) suggest a softer emission mechanism, allowing the intact emission of non-covalent lysozyme clusters, with reduced denaturation. Concerning the comparison with transfer experiments, there is also the possibility that denatured proteins might rearrange their conformation upon landing (with the substrate acting as an internal energy sink) or when placed in contact with the aqueous solution for the bioassay. Further work should explore the size limit of the molecules that could be transferred in the gas phase. The emission of lysozyme pentamers and hexamers in these simulations, and larger polystyrene molecules in a previous study [35], indeed suggest that significantly heavier molecules might be desorbed without fragmentation.

The *E/n* dependence of the fragmentation was also abundantly reported in the literature, both in MS and transfer experiments [18]. The experimental MS induced by $Ar^+_{1500\text{-}5000}$ clusters impinging on a "thick" lysozyme coating (several μm) with a total energy of 10 keV is reported in **Figure S14**. Though ionization plays a part, similar series of peaks appear below 200 Da, which tend to increase in intensity when *E/n* increases. Our simulation data, much like the experiments, show preferential cleavage sites on the proteins, producing specific fragments for the decomposition of the lysozyme (**Figure S12**). For example, in the case of fragments in the low-mass range (<200 Da), the peaks in the mass distribution of $E/n = 4.0$ eV/atom, also appear in the distributions of $E/n = 6.0$ and 10.0 eV/atom. In the MD, there is a large gap in the mass distribution of fragments, between the low-mass range and the quasi-intact molecule at 14 kDa, which is also consistent with the MS, where the peaks vanish beyond a few hundred Da. The difference between the experimental and theoretical approaches, as the simulations also suggest, is the influence of the organic layer structure (e.g. thickness). Nevertheless, similarities in the MS peaks when changing the *E/n* are observed theoretically (**Figure S12**) and experimentally (**Figure S14**).

One significant difference between the experiment and simulated MS concerns the small gaseous species (<30 Da), where the experiment gives a single peak at 18 Da, related to H_2O^+ or NH_4^+ (even without delayed extraction). The difference might be explained by the loss of neutral gas in the vacuum chamber and, perhaps, an effect of the organic layer thickness. Previous MD investigations of hydrocarbon molecules

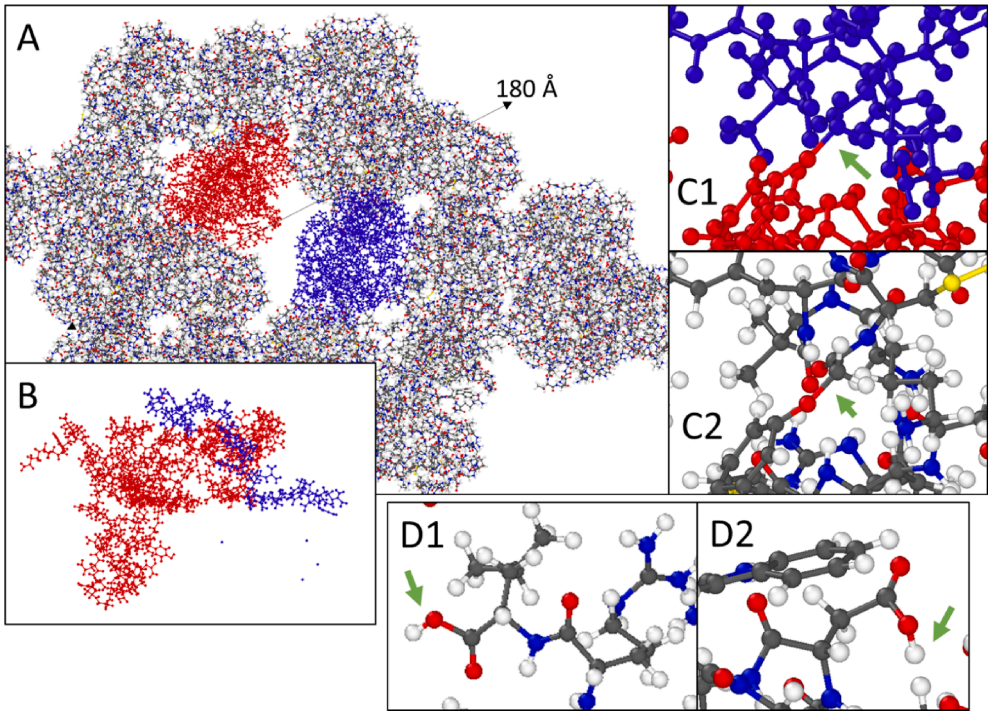

Fig. 10. Examples of reactions occurring upon Ar_{3000} impact (4.0 eV/atom) on an organic monolayer of lysozymes adsorbed on gold. A) Initial structure highlighting two lysozymes in red and blue; B) Final structure highlighting one lysozyme (red) and one fragment (blue); C) Highlight of the formation of a CO bond that connects a lysozyme (red) with a fragment (blue); D) Formation of HO bonds due to the migration of H from an external protein. Color code: H is white, C is gray, N is blue, O is red, S is yellow.

and polymers using the (AI)REBO potential also predicted very large numbers of stable C_2H_2 molecules [75]. There could also be a minor effect of the oscillations in the simulation results, where due to the distance cutoff for bound counting, some small fragments might be counted as new fragments instead of belonging to a bigger molecule.

Statistically, the reactions during the Ar cluster collision should change accordingly to the position and orientation of the proteins. In this study, we observed that the reactions mainly occur with the atoms that directly suffer the impact of the Ar cluster, i.e. at the interface between the Ar cluster and the lysozyme (Fig. 3). Compared with a bulk organic sample, the interaction with the gold surface also affects the reactions for two reasons: (i) the Ar atoms that scatter on the Au substrate, reflect more kinetic energy to the protein; (ii) the protein atoms which are compressed on the defects of the gold surface, have a higher probability to break bonds. A similar effect of increasing fragmentation near a hard interface was observed for thin polymeric layers adsorbed on ultra-flat silicon wafers (⟨100⟩ monocrystal surfaces)[74].

In some cases, the gold surface is disturbed by the impact. But significant plastic deformations only penetrate the slab when E/n reaches 10.0 eV/atom (**Figure S15**), creating bulk defects and mixing atoms from different layers. The amorphized region then reconstructs over time. However, even for lower energies, surface defects are created by the collision and they increase in number with E/n. Although the effect of the deposited energy density unit per area was not evaluated in this study, because of the high cost of computing full lysozymes, it is another parameter of the Ar cluster bombardment that can affect surface deformation, cratering and sputtering in inorganic and organic surfaces [11,76,77].

When elastic deformation dominates, one may wonder whether the pressure waves generated by the large Ar cluster and the elastic reaction of the gold crystal may influence the desorption process. Once the cluster hits the surface and induces a pressure wave, its propagation in the slab can be traced by the velocity perpendicular to the surface, as described by Postawa et. al [78] (**Figure S16**). Upon 6 eV/atom Ar_{3000} impact, the pressure wave propagation reaches the Langevin damping region at 500 fs (blue atoms, **Figure S16**), in agreement with the average velocity profile over time (dashed red line, **Figure S16E**). When a possible back propagation of the pressure wave or relaxation of the elastic wave (red atoms, **Figure S16**) hits the surface at 1500 fs, the protein is already desorbed. The oscillation in the velocity profile suggests that a period of elastic relaxation takes place instead of a pressure wave back propagation after the pressure wave hits the frozen bottom layers. On the one hand, the amplitude of velocity waves affects more the upper layer, while in the Langevin damping layers, the average velocity has a small amplitude (**Figure S16**). On the other hand, when the pressure wave reaches the frozen layer (500 fs), the intensity of the vibration wave tends to be unaffected. Thus we consider that the elastic waves dominate over the pressure wave back propagation. Concerning the lysozyme desorption process, the fact that the upward moving gold atoms (in red) are far behind the desorbing lysozyme in **Figure S16D** demonstrates that the surface oscillation does not participate to the protein ejection. Gold atoms can be removed from the surface to associate with the emitted protein fragments (**Figure S13**), due to the interaction between Au and S. The presence of Au atoms in desorbed proteins has also been observed experimentally [79].

Finally, from the methodological viewpoint, the effect of the nature of the repulsive part of the interatomic potentials (**Figure S1**) on our simulation results was evaluated. As an example, the time evolution of the number of lysozyme fragments is shown in **Figure S17** for an Ar_{3000} cluster impact with 6 eV/atom, with or without ZBL potential (see the Methods section). The time evolution is identical in the beginning (higher energy part of the interaction), and varies slightly afterward, with somewhat more fragments in the first 10 ps with pure ReaxFF, and a crossing of the curves at 10 ps, leading to a final cumulated fragment number that is larger with ReaxFF+ZBL at 20 ps. The energy distributions between the protein, Ar atoms and the slab at 10 ps, display very similar values for the simulation with pure ReaxFF and ReaxFF+ZBL (**Figure S18**). In addition, the slightly different evolution after 10 ps corresponds to low-energy unimolecular dissociation reactions that should be adequately described by pure ReaxFF. Upon examination of the interatomic potential energy curves, one can see that the repulsive energy barriers using ZBL tend to be overestimated with respect to DFT (some shown in **Figure S1**) and start at larger pair distances, while in pure ReaxFF they tend to be underestimated. However, the difference in behavior after 10 ps can hardly be attributed to that "high-energy" part of the potential, rather to the stochastic nature of the interaction where small changes of parameters can cause variations in the results. The observed variations may not seem negligible in absolute terms, giving us some limits in terms of quantification, but they do not affect the qualitative trends observed as a function of E and E/n in our results for a number of trajectories (15 for the single lysozyme on Au system). Another effect that is also observed with the ZBL repulsive barrier is the collision induced diffusion of H atoms in the gold slab, as was shown in **Figure S3**. To conclude, if the use of ZBL becomes crucial for higher energy (per atom) simulations, the collected data indicate that its necessity is reduced at the low collision energies used in our simulations, and may even suggest that it could add new artifacts in the results.

4. Conclusion

Our MD simulations predict that lysozymes (14 kDa) can be desorbed from a gold surface as well as from an organic thin film using large Ar clusters, when the total translational energy is larger than one kiloelectronvolt. For single lysozymes adsorbed on gold, molecular fragmentation depends mainly on the atomistic kinetic energy of the Ar cluster (E/n), but it is also promoted by the cluster size, arguably because the number of Ar atoms in the high-end of the energy distribution after impact is proportional to the cluster size and because the Ar atom correlated motion is already largely lost when they interact with the molecule. When the atomistic kinetic energy of the Ar cluster is $\leq$2.0 eV/atom, extensive molecular dissociation is not observed, only occasional H abstraction reactions, in good agreement with recent experiments which demonstrated intact molecular transfer for the same energy range.

The structure and thickness of the adsorbed biological material influence the desorption of proteins. In a thicker layer (bilayer versus monolayer), more proteins are removed and they are generally less fragmented for the same cluster impact conditions. Nevertheless, an increase of fragmentation with E/n and cluster size are also observed in the lysozyme monolayer, as in the single adsorbed molecule. Therefore, the single molecule on gold remains a good qualitative model to study fragmentation and its mechanisms. Additionally, in the monolayer, the number of desorbed molecules increases with the cluster size. The desorption of non-covalent clusters (up to the hexamer) from a lysozyme bilayer upon 15 keV Ar_{5000} bombardment, with limited molecular denaturation, confirms that the molecular environment favors soft desorption in comparison with the hard substrate.

These results open perspectives for investigating the desorption and transfer of heavier intact biomolecules in the vacuum using large gas clusters with controlled kinetic energies or electrosprayed droplets. In transfer experiments, one might consider the fabrication of new multilayered architectures involving larger proteins (enzymes) or even antibodies. In secondary ion mass spectrometry, one could expand the analytical mass range for biomolecules provided that (i) an efficient intrinsic ionization mechanism exists - or an external ionization can be implemented - for the desorbing molecules and (ii) the detection scheme is adapted for such high mass species.

Declaration of Competing Interest

The authors declare that they have no known competing financial interests or personal relationships that could have appeared to influence

the work reported in this paper.

Data availability

Data will be made available on request.

Acknowledgments

The authors wish to thank V. Delmez and B. Tomasetti for the experimental data provided in supplementary information. S.B. would like to acknowledge the “Fonds National de la Recherche Scientifique” (FNRS) for financing the project “Cluster-protein impacts” under the convention PDR T.0052.22. Additional funding was provided by the Fédération Wallonie Bruxelles, through the project "iBeam" (ARC convention N° 18/23-090). A.D. is a Research Director of FNRS. Computational resources were provided by the Institut de Calcul Intensif et de Stockage de Masse (CISM) at Université Catholique de Louvain.

Appendix A. Supplementary data

Supplementary data to this article can be found online at https://doi.org/10.1016/j.apsusc.2023.157487.

References

[1] P. Kebarle, U.H. Verkerk, Electrospray: from ions in solution to ions in the gas phase, what we know now, Mass Spectrom. Rev. 28 (2009) 898–917.
[2] I.S. Gilmore, S. Heiles, C.L. Pieterse, Metabolic imaging at the single-cell scale: recent advances in mass spectrometry imaging, Annu. Rev. Anal. Chem. 12 (2019) 201–224.
[3] R.M.A. Heeren, Getting the picture: The coming of age of imaging MS, Int. J. Mass Spectrom. 377 (2015) 672–680.
[4] J.A. Camarero, Recent developments in the site-specific immobilization of proteins onto solid supports, Pept. Sci. 90 (2008) 450–458.
[5] R. Yang, A. Asatekin, K.K. Gleason, Design of conformal, substrate-independent surface modification for controlled protein adsorption by chemical vapor deposition (CVD), Soft Matter 8 (2012) 31–43.
[6] I. Jacquemart, E. Pamuła, V.M. de Cupere, P.G. Rouxhet, C.C. Dupont-Gillain, Nanostructured collagen layers obtained by adsorption and drying, J. Colloid Interface Sci. 278 (2004) 63–70.
[7] F.A. Denis, P. Hanarp, D.S. Sutherland, J. Gold, C. Mustin, P.G. Rouxhet, Y. F. Dufrêne, Protein adsorption on model surfaces with controlled nanotopography and chemistry, Langmuir 18 (2002) 819–828.
[8] P.J. Wilde, Interfaces: their role in foam and emulsion behaviour, Curr. Opin. Colloid Interface Sci. 5 (2000) 176–181.
[9] F.A. Denis, A. Pallandre, B. Nysten, A.M. Jonas, C.C. Dupont-Gillain, Alignment and assembly of adsorbed collagen molecules induced by anisotropic chemical nanopatterns, Small 1 (2005) 984–991.
[10] D. Falconnet, G. Csucs, H.M. Grandin, M. Textor, Surface engineering approaches to micropattern surfaces for cell-based assays, Biomaterials 27 (2006) 3044–3063.
[11] A. Delcorte, V. Delmez, C. Dupont-Gillain, C. Lauzin, H. Jefford, M. Chundak, C. Poleunis, K. Moshkunov, Large cluster ions: soft local probes and tools for organic and bio surfaces, PCCP 22 (2020) 17427–17447, https://doi.org/10.1039/D0CP02398A.
[12] T. Mouhib, C. Poleunis, N. Wehbe, J.J. Michels, Y. Galagan, L. Houssiau, P. Bertrand, A. Delcorte, Molecular depth profiling of organic photovoltaic heterojunction layers by ToF-SIMS: comparative evaluation of three sputtering beams, Analyst 138 (2013) 6801–6810.
[13] A.S. Mohammadi, N.T.N. Phan, J.S. Fletcher, A.G. Ewing, Intact lipid imaging of mouse brain samples: MALDI, nanoparticle-laser desorption ionization, and 40 keV argon cluster secondary ion mass spectrometry, Anal. Bioanal. Chem. 408 (2016) 6857–6868.
[14] M.K. Passarelli, A. Pirkl, R. Moellers, D. Grinfeld, F. Kollmer, R. Havelund, C. F. Newman, P.S. Marshall, H. Arlinghaus, M.R. Alexander, The 3D OrbiSIMS—label-free metabolic imaging with subcellular lateral resolution and high mass-resolving power, Nat. Methods 14 (2017) 1175–1183.
[15] K. Mochiji, M. Hashinokuchi, K. Moritani, N. Toyoda, Matrix-free detection of intact ions from proteins in argon-cluster secondary ion mass spectrometry, Rapid Communications in Mass Spectrometry: An International Journal Devoted to the Rapid Dissemination of Up-to-the-Minute Research in Mass Spectrometr. 23 (2009) 648–652.
[16] S. Oshima, I. Kashihara, K. Moritani, N. Inui, K. Mochiji, Soft-sputtering of insulin films in argon-cluster secondary ion mass spectrometry, Rapid Commun. Mass Spectrom. 25 (2011) 1070–1074.
[17] A.M. Kotowska, G.F. Trindade, P.M. Mendes, P.M. Williams, J.W. Aylott, A. G. Shard, M.R. Alexander, D.J. Scurr, Protein identification by 3D OrbiSIMS to facilitate in situ imaging and depth profiling, Nat. Commun. 11 (2020) 5832.
[18] V. Delmez, B. Tomasetti, T. Daphnis, C. Poleunis, C. Lauzin, C. Dupont-Gillain, A. Delcorte, Gas Cluster Ion Beams as a Versatile Soft-Landing Tool for the Controlled Construction of Thin (Bio) Films, ACS Appl. Bio Mater. 5 (2022) 3180–3192.
[19] V. Delmez, H. Degand, C. Poleunis, K. Moshkunov, M. Chundak, C. Dupont-Gillain, A. Delcorte, Deposition of Intact and Active Proteins In Vacuo Using Large Argon Cluster Ion Beams, J. Phys. Chem. Lett. 12 (2021) 952–957, https://doi.org/10.1021/acs.jpclett.0c02510.
[20] A. Delcorte, C. Poleunis, Mechanistic insight into gas cluster-induced sputtering of kilodalton molecules using kinetic energy distribution measurements, J. Phys. Chem. C 123 (2019) 19704–19714.
[21] T. Fu, S. Della-Negra, D. Touboul, A. Brunelle, Internal energy distribution of secondary ions under argon and bismuth cluster bombardments:“soft” versus “hard” desorption–ionization process, J. Am. Soc. Mass Spectrom. 30 (2018) 321–328.
[22] S. Ninomiya, Y. Nakata, K. Ichiki, T. Seki, T. Aoki, J. Matsuo, Measurements of secondary ions emitted from organic compounds bombarded with large gas cluster ions, Nucl. Instrum. Methods Phys. Res. B 256 (2007) 493–496.
[23] C.L. Cleveland, U. Landman, Dynamics of cluster-surface collisions, Science 257 (1992) (1979) 355–361.
[24] F. Musumeci, H. Ryuto, A. Sakata, M. Takeuchi, G.H. Takaoka, Spectroscopic evidences of high temperatures and pressures during the cluster ion beam interaction with solid surfaces, J. Lumin. 172 (2016) 224–230.
[25] B.J. Garrison, A. Delcorte, K.D. Krantzman, Molecule liftoff from surfaces, Acc. Chem. Res. 33 (2000) 69–77.
[26] Z. Postawa, R. Paruch, L. Rzeznik, B.J. Garrison, Dynamics of large Ar cluster bombardment of organic solids, Surface and Interface Analysis. 45 (2013) 35–38. https://doi.org/https://doi.org/10.1002/sia.4927.
[27] N. Tuccitto, D. Maciazek, Z. Postawa, A. Licciardello, MD-based transport and reaction model for the simulation of SIMS depth profiles of molecular targets, J. Phys. Chem. C 123 (2019) 20188–20194.
[28] A. Delcorte, B.J. Garrison, K. Hamraoui, Dynamics of molecular impacts on soft materials: from fullerenes to organic nanodrops, Anal. Chem. 81 (2009) 6676–6686.
[29] M. Kanski, B.J. Garrison, Z. Postawa, Effect of oxygen chemistry in sputtering of polymers, J. Phys. Chem. Lett. 7 (2016) 1559–1562.
[30] P. Schneider, M. Dürr, Cluster-induced desorption investigated by means of molecular dynamics simulations—Microsolvation in clusters of polar and non-polar constituents, J. Chem. Phys. 150 (2019), 214301.
[31] T. Aoki, Molecular dynamics simulations of cluster impacts on solid targets: implantation, surface modification, and sputtering, J. Comput. Electron. 13 (2014) 108–121.
[32] J. Samela, K. Nordlund, Atomistic simulation of the transition from atomistic to macroscopic cratering, Phys. Rev. Lett. 101 (2008), 027601.
[33] L. Rzeznik, B. Czerwinski, B.J. Garrison, N. Winograd, Z. Postawa, Microscopic insight into the sputtering of thin polystyrene films on Ag 111 induced by large and slow Ar clusters, J. Phys. Chem. C 112 (2008) 521–531.
[34] C. Mücksch, C. Anders, H. Gnaser, H.M. Urbassek, Dynamics of L-phenylalanine sputtering by argon cluster bombardment, J. Phys. Chem. C 118 (2014) 7962–7970.
[35] A. Delcorte, A Microscopic View of Macromolecule Transfer in the Vacuum Using Gas and Bismuth Clusters, J. Phys. Chem. C 126 (2022) 7307–7318.
[36] H. Tian, D. Maciążek, Z. Postawa, B.J. Garrison, N. Winograd, CO2 cluster ion beam, an alternative projectile for secondary ion mass spectrometry, J. Am. Soc. Mass Spectrom. 27 (2016) 1476–1482.
[37] M. Kański, D. Maciazek, Z. Postawa, C.M. Ashraf, A.C.T. Van Duin, B.J. Garrison, Development of a charge-implicit ReaxFF potential for hydrocarbon systems, J. Phys. Chem. Lett. 9 (2018) 359–363.
[38] T.P. Senftle, S. Hong, M.M. Islam, S.B. Kylasa, Y. Zheng, Y.K. Shin, C. Junkermeier, R. Engel-Herbert, M.J. Janik, H.M. Aktulga, The ReaxFF reactive force-field: development, applications and future directions, NPJ Comput. Mater. 2 (2016) 1–14.
[39] K. Chenoweth, A.C.T. van Duin, W.A. Goddard, ReaxFF reactive force field for molecular dynamics simulations of hydrocarbon oxidation, J. Phys. Chem. A 112 (2008) 1040–1053.
[40] S.J. Stuart, A.B. Tutein, J.A. Harrison, A reactive potential for hydrocarbons with intermolecular interactions, J. Chem. Phys. 112 (2000) 6472–6486.
[41] A.C.T. van Duin, S. Dasgupta, F. Lorant, W.A. Goddard, ReaxFF: a reactive force field for hydrocarbons, J. Phys. Chem. A 105 (2001) 9396–9409.
[42] M.A. Wood, A.C.T. van Duin, A. Strachan, Coupled thermal and electromagnetic induced decomposition in the molecular explosive αHMX; a reactive molecular dynamics study, J. Phys. Chem. A 118 (2014) 885–895.
[43] E.C. Neyts, A.C.T. van Duin, A. Bogaerts, Insights in the plasma-assisted growth of carbon nanotubes through atomic scale simulations: effect of electric field, J. Am. Chem. Soc. 134 (2012) 1256–1260.
[44] S. Bertolini, P.B. Balbuena, Buildup of the Solid Electrolyte Interphase on Lithium-Metal Anodes: Reactive Molecular Dynamics Study, J. Phys. Chem. C 122 (2018) 10783–10791, https://doi.org/10.1021/acs.jpcc.8b03046.
[45] W. Zhang, A.C.T. van Duin, Improvement of the ReaxFF description for functionalized hydrocarbon/water weak interactions in the condensed phase, J. Phys. Chem. B 122 (2018) 4083–4092.
[46] S. Monti, A. Corozzi, P. Fristrup, K.L. Joshi, Y.K. Shin, P. Oelschlaeger, A.C.T. van Duin, V. Barone, Exploring the conformational and reactive dynamics of biomolecules in solution using an extended version of the glycine reactive force field, PCCP 15 (2013) 15062–15077.

[47] S. Monti, C. Li, H. Ågren, V. Carravetta, Dropping a droplet of cysteine molecules on a rutile (110) interface: Reactive versus nonreactive classical molecular dynamics simulations, J. Phys. Chem. C 119 (2015) 6703–6712.
[48] S. Monti, G. Barcaro, L. Sementa, V. Carravetta, H. Ågren, Dynamics and self-assembly of bio-functionalized gold nanoparticles in solution: Reactive molecular dynamics simulations, Nano Res. 11 (2018) 1757–1767.
[49] S. Bertolini, T. Jacob, Valence energy correction for electron reactive force field, J. Comput. Chem. 43 (2022) 870–878.
[50] M.M. Islam, G. Kolesov, T. Verstraelen, E. Kaxiras, A.C.T. van Duin, eReaxFF: a pseudoclassical treatment of explicit electrons within reactive force field simulations, J. Chem. Theory Comput. 12 (2016) 3463–3472.
[51] M.M. Islam, A.C.T. van Duin, Reductive decomposition reactions of ethylene carbonate by explicit electron transfer from lithium: an eReaxFF molecular dynamics study, J. Phys. Chem. C 120 (2016) 27128–27134.
[52] L. Liu, Y. Liu, S. v Zybin, H. Sun, W.A. Goddard, ReaxFF-lg: Correction of the ReaxFF Reactive Force Field for London Dispersion, with Applications to the Equations of State for Energetic Materials, J Phys Chem A. 115 (2011) 11016–11022. https://doi.org/10.1021/jp201599t.
[53] M. Refaee, T. Tezuka, K. Akasaka, M.P. Williamson, Pressure-dependent Changes in the Solution Structure of Hen Egg-white Lysozyme, J. Mol. Biol. 327 (2003) 857–865, https://doi.org/10.1016/S0022-2836(03)00209-2.
[54] A.P. Thompson, H.M. Aktulga, R. Berger, D.S. Bolintineanu, W.M. Brown, P.S. Crozier, P.J. in 't Veld, A. Kohlmeyer, S.G. Moore, T.D. Nguyen, R. Shan, M.J. Stevens, J. Tranchida, C. Trott, S.J. Plimpton, LAMMPS - a flexible simulation tool for particle-based materials modeling at the atomic, meso, and continuum scales, Comput Phys Commun. 271 (2022) 108171. https://doi.org/https://doi.org/10.1016/j.cpc.2021.108171.
[55] H.M. Aktulga, C. Knight, P. Coffman, K.A. O'Hearn, T.-R. Shan, W. Jiang, Optimizing the performance of reactive molecular dynamics simulations for many-core architectures, Int. J. High Perform Comput. Appl. 33 (2019) 304–321.
[56] W.J. Mortier, S.K. Ghosh, S. Shankar, Electronegativity-equalization method for the calculation of atomic charges in molecules, J. Am. Chem. Soc. 108 (1986) 4315–4320.
[57] S. Monti, V. Carravetta, H. Ågren, Simulation of gold functionalization with cysteine by reactive molecular dynamics, J. Phys. Chem. Lett. 7 (2016) 272–276.
[58] A.M. Kamat, A.C.T. Van Duin, A. Yakovlev, Molecular dynamics simulations of laser-induced incandescence of soot using an extended ReaxFF reactive force field, J. Phys. Chem. A 114 (2010) 12561–12572.
[59] C. Anders, H.M. Urbassek, Impacts into cosmic ice surfaces: A molecular-dynamics study using the Reax force field, Nucl. Instrum. Methods Phys. Res. B 303 (2013) 200–204.
[60] J.F. Ziegler, J.P. Biersack, U. Littmark, The stopping and ranges of ions in solids, Vol. 1, The Stopping and Ranges of Ions in Matter. (1985).
[61] M. Kański, D. Maciążek, Z. Postawa, C.M. Ashraf, A.C.T. van Duin, B.J. Garrison, Development of a Charge-Implicit ReaxFF Potential for Hydrocarbon Systems, J. Phys. Chem. Lett. 9 (2018) 359–363, https://doi.org/10.1021/acs.jpclett.7b03155.
[62] M.P. Seah, S.J. Spencer, A.G. Shard, Angle dependence of argon gas cluster sputtering yields for organic materials, J. Phys. Chem. B 119 (2015) 3297–3303.
[63] M.P. Seah, R. Havelund, I.S. Gilmore, Universal equation for argon cluster size-dependence of secondary ion spectra in SIMS of organic materials, J. Phys. Chem. C 118 (2014) 12862–12872.
[64] S. Nosé, A unified formulation of the constant temperature molecular dynamics methods, J. Chem. Phys. 81 (1984) 511–519.
[65] N. Shuichi, Constant temperature molecular dynamics methods, Prog. Theor. Phys. Suppl. 103 (1991) 1–46.
[66] D.M. Bylander, L. Kleinman, Energy fluctuations induced by the Nosé thermostat, Phys. Rev. B 46 (1992) 13756.
[67] T. Schneider, E. Stoll, Molecular-dynamics study of a three-dimensional one-component model for distortive phase transitions, Phys. Rev. B 17 (1978) 1302.
[68] B. Dünweg, W. Paul, Brownian dynamics simulations without Gaussian random numbers, Int. J. Mod. Phys. C 2 (1991) 817–827.
[69] D.L. Burke, A.P. O'Mullane, V.E. Lodge, M.B. Mooney, Auto-inhibition of hydrogen gas evolution on gold in aqueous acid solution, J. Solid State Electrochem. 5 (2001) 319–327.
[70] A.O. Gezerman, B.D. Çorbacıoğlu, Development of alternative environment friendly nickel and gold plating baths, Surf. Eng. 31 (2015) 641–649.
[71] Y. Arata, Y.-C. Zhang, Sono implantation of hydrogen and deuterium from water into metallic fine powders, Appl. Phys. Lett. 76 (2000) 2472–2474.
[72] L. Stobiński, R. Duś, Atomic hydrogen solubility in thin gold films and its influence on hydrogen thermal desorption spectra from the surface, Appl. Surf. Sci. 62 (1992) 77–82.
[73] T.B. Flanagan, D. Wang, Hydrogen permeation through fcc Pd–Au alloy membranes, J. Phys. Chem. C 115 (2011) 11618–11623.
[74] V. Cristaudo, C. Poleunis, P. Laha, P. Eloy, T. Hauffman, H. Terryn, A. Delcorte, Ion yield enhancement at the organic/inorganic interface in SIMS analysis using Ar-GCIB, Appl. Surf. Sci. 536 (2021), 147716.
[75] A. Delcorte, B.J. Garrison, Kiloelectronvolt argon-induced molecular desorption from a bulk polystyrene solid, J. Phys. Chem. B 108 (2004) 15652–15661.
[76] T. Aoki, T. Seki, J. Matsuo, Study of density effect of large gas cluster impact by molecular dynamics simulations, Nucl. Instrum. Methods Phys. Res. B 267 (2009) 2999–3001, https://doi.org/10.1016/j.nimb.2009.06.019.
[77] A. Delcorte, M. Debongnie, Macromolecular sample sputtering by large Ar and CH4 clusters: elucidating chain size and projectile effects with molecular dynamics, J. Phys. Chem. C 119 (2015) 25868–25879.
[78] Z. Postawa, B. Czerwinski, M. Szewczyk, E.J. Smiley, N. Winograd, B.J. Garrison, Enhancement of sputtering yields due to C60 versus Ga bombardment of Ag 111 as explored by molecular dynamics simulations, Anal Chem. 75 (2003) 4402–4407.
[79] B. Simões, W.J. Guedens, C. Keene, K. Kubiak-Ossowska, P. Mulheran, A. M. Kotowska, D.J. Scurr, M.R. Alexander, A. Broisat, S. Johnson, S. Muyldermans, N. Devoogdt, P. Adriaensens, P.M. Mendes, Direct Immobilization of Engineered Nanobodies on Gold Sensors, ACS Appl. Mater. Interfaces 13 (2021) 17353–17360, https://doi.org/10.1021/acsami.1c02280.